NPL
National Physical Laboratory

NPL REPORT IR 62

FEATURES OF THE NEUTRON SPECTRA PRODUCED USING TRITIUM TARGETS CURRENTLY AVAILABLE FOR NEUTRON PRODUCTION WITH THE T(d,n)^{4}He REACTION AT NPL - JUNE 2022

DAVID J. THOMAS AND MICHAEL BUNCE

SEPTEMBER 2022

Features of the neutron spectra produced using tritium targets currently available for neutron production with the T(d,n)^{4}He reaction at NPL - June 2022

David J. Thomas and Michael Bunce
Nuclear Metrology Group

ABSTRACT

Targets consisting of tritium absorbed in thin layers of titanium are used at NPL to produce neutrons via the T(d,n)^{4}He reaction. Deuteron beams are produced using the NPL 3.5 MV Van de Graaff accelerator, and up until recently this accelerator could not operate at potentials below about 1 MeV. Recent changes have, however, allowed lower voltage operation and the production of deuterium beams down to about 500 keV. This, and the fact that a new tritium target with higher tritium content is available, have initiated an investigation of the neutron spectra now achievable with the T(d,n)^{4}He reaction. These are documented in this report which also includes an investigation of the most appropriate fluence to dose equivalent conversion factors to use for these spectra.

© NPL Management Limited, 2022

ISSN 1754-2952

https://doi.org/10.47120/npl.IR62

National Physical Laboratory
Hampton Road, Teddington, Middlesex, TW11 0LW

Extracts from this report may be reproduced provided the source is acknowledged and the extract is not taken out of context.

Approved on behalf of NPLML by
Ben Russell, Science Leader – Nuclear Metrology

GLOSSARY

BIPM Bureau International des Poids et Mesures

CCRI Consultative Committee for Ionizing Radiation (Comité consultatif des rayonnements ionisants)

ICRU International Commission on Radiation Units and Measurements

ISO International Organization for Standardization

JRC Joint Research Centre

PTB Physikalisch-Technische Bundesanstalt - the German national metrology lab

CONTENTS

1. Introduction

As of June 2022, there are three tritium targets commonly used, or available for use, for d-T neutron production at NPL. All three were made by the French company Sodern. The properties of these targets, and the blank targets that can be used for investigating target-backing neutrons, are shown in Table 1.

Table 1. Characteristics of tritium targets available in June 2022 for d-T neutron production at NPL.

Name	Production or shipping date*	Target or blank	History	Nominal titanium thickness (μg cm^{-2})	Actual titanium thickness (μg cm^{-2})	Original T to Ti ratio	Current T to Ti ratio	Current tritium activity (GBq)	Backing material
CIRM 04	22/11/2005	Target	In use	1000	943	1.62	0.64	68.6	Au
CIRM 08	27/05/2008	Blank	In use	1000	935	-	-	-	Au
NPL 09	04/11/2014	Target	In use	600	614	1.59	1.04	72.5	Au
NPL 13	06/12/2021	Target	Unused	1500	#	1.40	1.36	232	Ag
NPL 14	06/12/2021	Blank	Unused	1500	#	-	-	-	Ag

* The actual production date, or the date the tritium activity was determined is seldom known, and the shipping date can sometimes be the best estimate available of the production date.

No value provided by Sodern. Actual tritium thickness assumed to be same as the nominal value.

There is one additional Sodern target available. This is CIRM 03, but it is both old, about 20 years, and has a thin titanium layer of 355 μg cm^{-2}. The current tritium activity is about 8.6 GBq, c.f. 232 GBq for the most active target in Table 1. CIRM 03 can still be used, but the output is low compared to the other three, so is seldom used nowadays. Earlier targets, produced by UKAEA Harwell, and dating back to at least the 1970s are not considered here, being so old the yield is extremely low. One target from this period, Gtu 772, is still available and could be used for very low intensity irradiations. The titanium layer is thin, 355 μg cm^{-2}, so the neutron energy distribution is narrow, but the tritium activity is now down to 2.2 GBq.

For all the Sodern targets the titanium covers a circular area 25.4 mm in diameter. The backing disc is 0.5 mm thick and 38 mm in diameter, and the target disc is held on the end of the dedicated tritium target can by suction – see Figure 1.

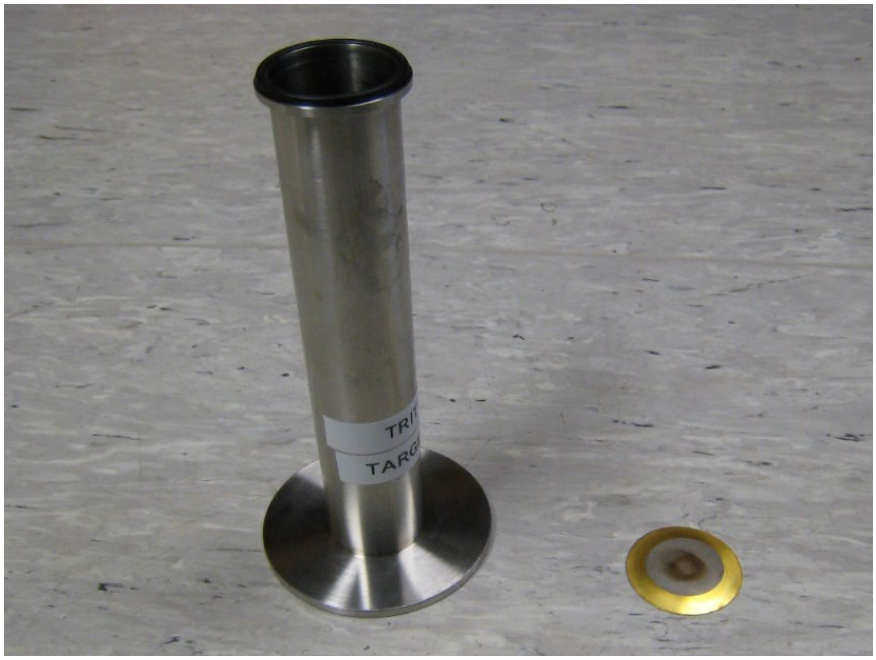

Figure 1. Target can used for tritium targets and a typical gold backed tritium target.

The recent installation of the PTB corona discharge unit on the NPL Van de Graaff has opened up options for lower terminal voltages, and hence the production of lower energy d-T neutron fields at 0° to the deuteron beam. With the previous corona unit, the lowest deuteron energy was about 940 keV, which produces 16.5 MeV neutrons at 0°, but with the new unit deuteron energies down to 500 keV are possible. This report investigates the neutron spectra now available using deuteron beams with energies below 1 MeV and also investigates the options for higher energy neutrons with these targets.

ISO Standard 8529-1[(1)] recommends monoenergetic energies for device calibrations and in addition to 14.8 MeV, the energy produced by the d-T reaction using deuteron beams in the 100 to 200 keV region, it includes 19 MeV. This is easily produced at NPL using the d-T reaction, requiring a deuteron beam energy of about 2.6 MeV, and although this energy has been used for cross section measurements at NPL in the past, it is not generally used for device calibrations because of problems with contaminant neutron production by deuterons of this energy. Nevertheless, it has been chosen as an energy to be included in a forthcoming BIPM CCRI key comparison (CCRI(III)-K12), so information is also presented on the spectra obtained when these targets are used to produce 19 MeV neutrons. The next version of ISO Standard 8529-1 will include 17 MeV as a recommended energy, so data are also presented for this energy.

2. Characteristics of d-T fields achievable at 0°

The EU JRC program NeuSDesc[(2)] was used to predict the characteristics of the neutron fields achievable with the three Sodern targets listed in Table 1. For deuteron beams at and below 1 MeV four energies were chosen: 500 keV, 600 keV, 800 keV, and 1000 keV. For the production of neutrons with mean energies of 17 and 19 MeV the deuteron energy was chosen for each target in order to provide a neutron distribution with this mean energy.

Two of the targets, CIRM 04 and NPL 09, together with the blank target CIRM 08, have been used to produce neutrons using a deuteron beam with an energy of about 940 keV, so can in principle be used to produce neutrons with lower energy deuteron beams without being compromised by neutron production from d-D reactions in the layer of deuterons already deposited at the end of their range. Target NPL 13 and blank target NPL 14 are as yet unused, so could be employed to produce any chosen neutron energy, e.g., 19 MeV, although any subsequent change of use would have to involve a lower deuteron beam energy.

The spectra are shown in Figure 2 – NPL 09 with 614 µg cm^{-2} of titanium, Figure 3 – CIRM 04 with 943 µg cm^{-2} of titanium, and Figure 4 – NPL 13 with 1500 µg cm^{-2} of titanium. The quantity plotted is the 0° neutron fluence per MeV per µA of beam on the target, at a distance of 100 cm from the target.

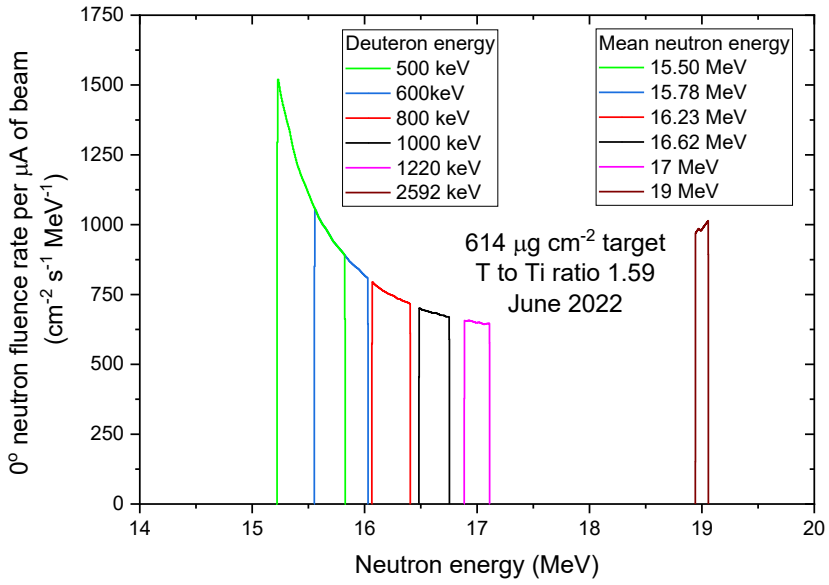

Figure 2. d-T spectra at various deuteron energies for a T:Ti target with Ti thickness of 614 µg cm^{-2}.

NeuSDesc can make allowance for finite detector size and for straggling of the deuterium beam in the target. The data shown in this section were, however, obtained directly from the user interface. They do not include these effects and are thus essentially for a point detector with no straggling.

It is important to note that the spectrum calculations were performed with the original T:Ti ratio listed in Table 1. The tritium decays to ^{3}He and there is evidence that this remains in the target layer, and hence contributes to the slowing down of the deuterium ions, and so influences the shape of the neutron spectrum. Using the original T:Ti ratio assumes the stopping power for ^{3}He is the same as for tritium, which may not be exact, but in the absence of a mixed tritium / ^{3}He target in NeuSDesc, this approach is preferable for calculating the spectrum to using the current T:Ti ratio, which would underestimate the slowing down. It does, however, give the yield as it was when the target was new. For calculating the current yield, the current T:Ti ratio must be used, and this has been done later in this report.

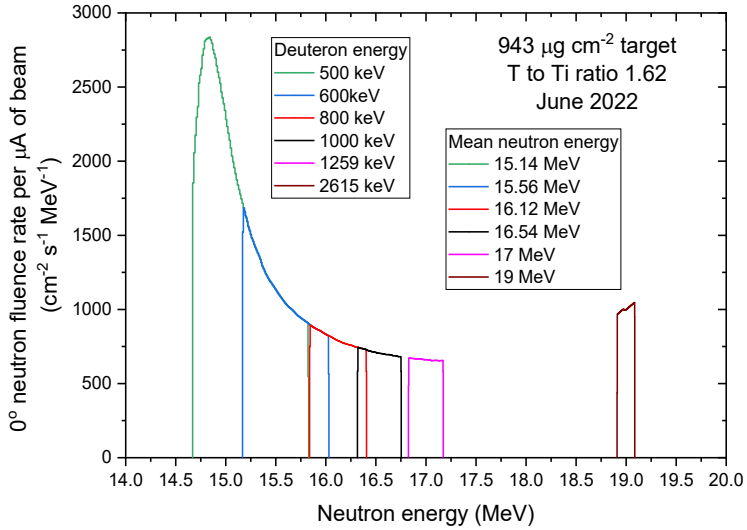

Figure 3. d-T spectra at various deuteron energies for a T:Ti target with Ti thickness of 943 µg cm^{-2}.

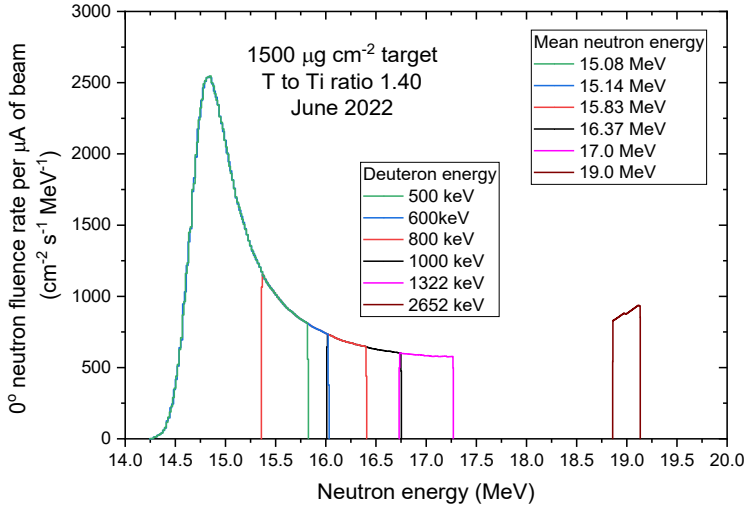

Figure 4. d-T spectra at various deuteron energies for a T:Ti target with Ti thickness of 1500 µg cm^{-2}.

The general features displayed in the plots are largely predictable from the properties of these targets, but the use of NeuSDesc has the advantage of making things quantitative. Thus, the mean neutron energy, as expected, decreases as the incident deuteron energy decreases below 1 MeV and, because the d-T cross section increases with decreasing energy from 1 MeV down to a peak at about 110 keV, the yield increases. For the thinner titanium layers, the beam traverses the layer and stops in the target backing for all the energies considered, but for the 1500 µg cm^{-2} target the 500 keV and 600 keV deuteron beams stop in the titanium layer.

Also plotted in the figures are the neutron distributions expected when the deuteron energy is set to provide neutrons with mean energies of 17 or 19 MeV. The yield at 19 MeV appears higher than at 17 MeV. This is the result of the 19 MeV neutrons being spread over a narrower range of energies. The total 17 MeV fluence is actually higher. As illustrated in Figure 5, the zero degree cross section has a shallow minimum at a deuteron energy of about 2.3 MeV[3,4], and increases up until about 6 MeV. However, it is higher in the 1.2-1.3 MeV region, the deuteron energy required for 17 MeV neutron production, than at 2.6 MeV, the energy required for 19 MeV neutrons. The 0° cross section is increasing with energy at 2.6 MeV, which explains the shape of the 19 MeV peak, i.e. with more neutrons on the high energy side than on the low energy side.

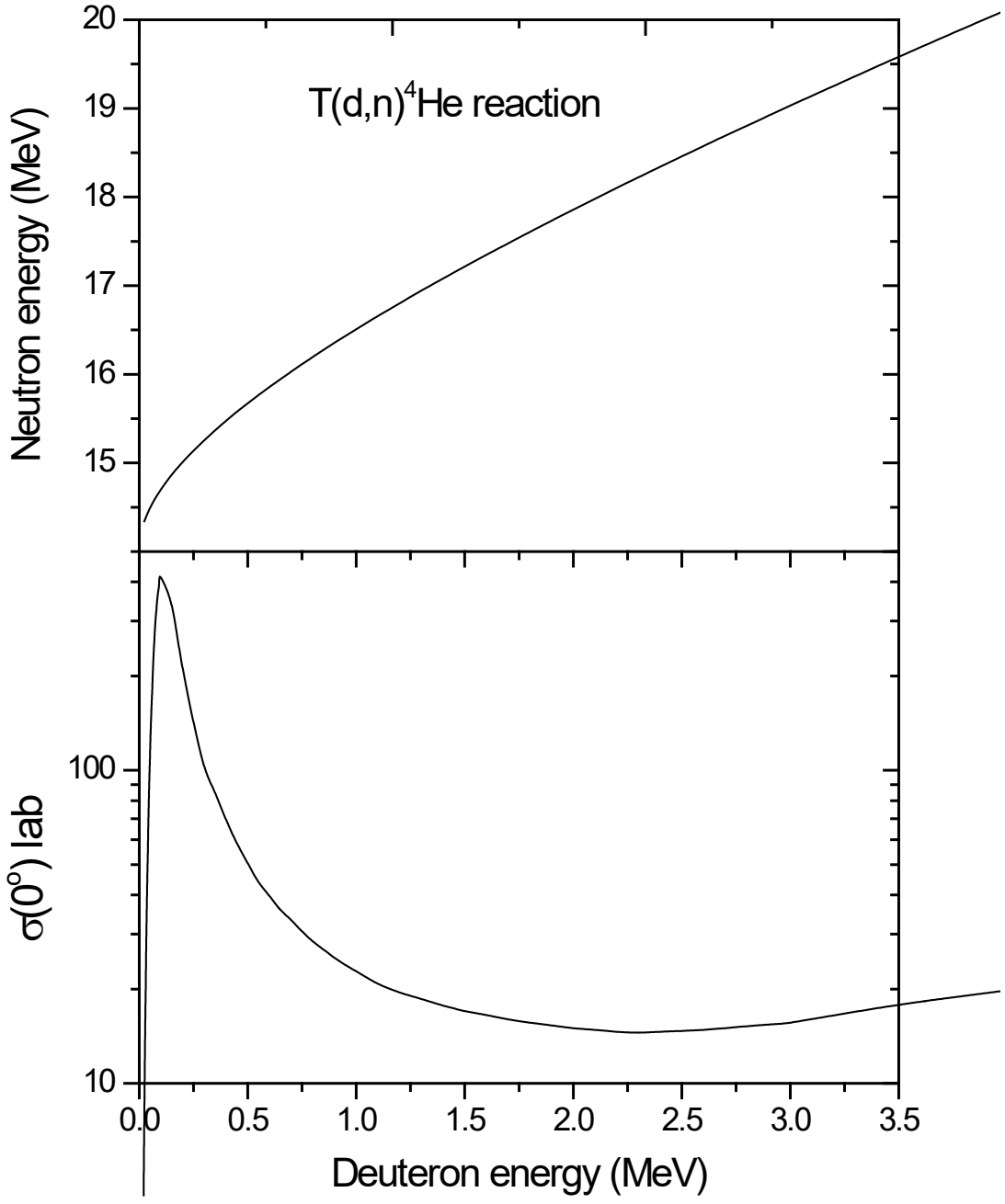

Figure 5. Zero degree cross section and neutron energy as a function of deuteron energy, data are from reference 3.

Neutron mean energies and the width of the neutron distribution are plotted in Figure 6 and Figure 7 respectively. The width plotted is the difference between the maximum and minimum energies as calculated by NeuSDesc.

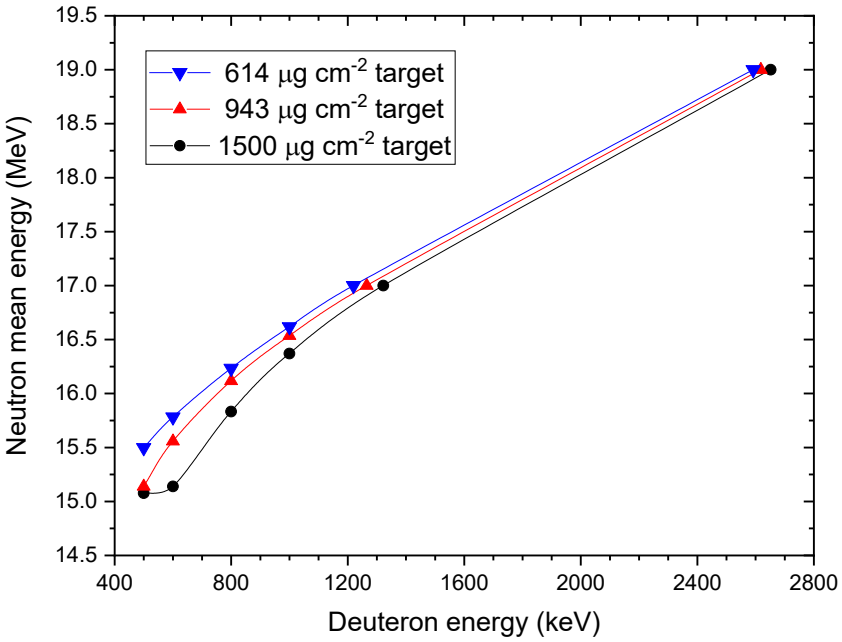

Figure 6. Mean neutron energies for the three targets as a function of deuteron energy.

As expected, the neutron mean energy is highest, at all deuteron bombarding energies, for the 614 μg cm^{-2} target where the deuteron energy loss in the titanium layer is least. The shape of the mean energy curve for the 943 μg cm^{-2} target is similar to that for the 614 μg cm^{-2} although the actual values are lower. For the 1500 μg cm^{-2} target the decrease in the neutron mean energy with decreasing deuteron bombarding energy slows down for the lowest beam energies because a large fraction of the neutrons is produced by deuterons with energies close to that for the peak of the T(d,n) cross section.

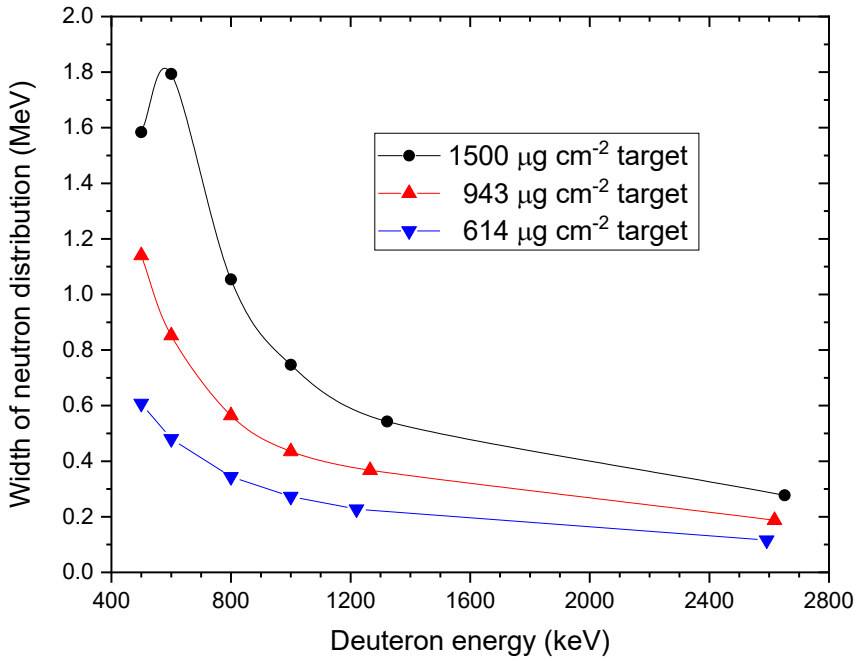

Figure 7. Total widths of the neutron energy distributions for the three targets.

For the full width of the neutron distribution, (maximum energy – minimum energy) as shown in Figure 7, the values increase with decreasing deuteron bombarding energy for both the 614 μg cm^{-2} and the 943 μg cm^{-2} targets. For the 1500 μg cm^{-2} target a similar pattern is seen until the width eventually starts to decrease at deuteron energies bellow the point where the beam stops in the titanium layer.

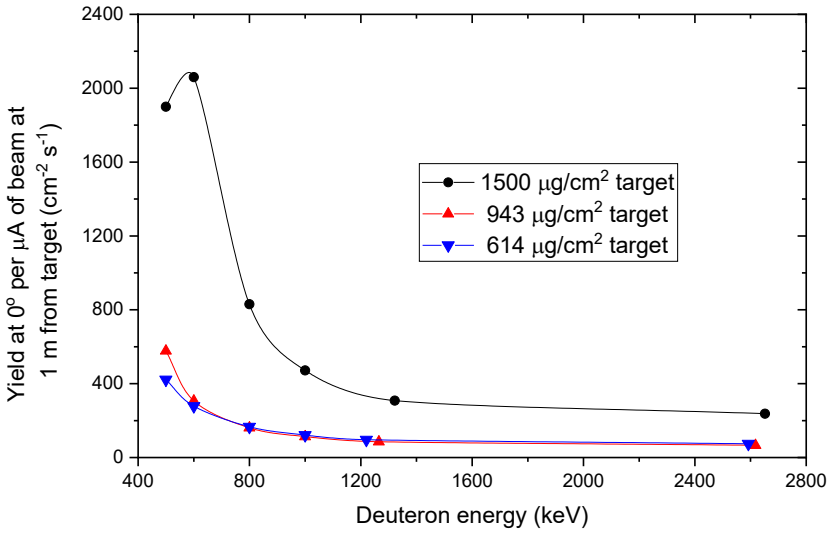

Figure 8. Variation of the total 0° yield as a function of deuteron bombarding energy for the 3 targets.

Figure 8 shows how the total neutron yield varies with deuteron bombarding energy for the three targets. The amount of tritium in each titanium target layer in June 2022 was used. This was estimated by decaying the original T:Ti ratio supplied by the manufacturer using the 12.32 year half-life of tritium[a]. (The T:Ti ratio and the titanium layer thickness are the quantities used by NeuSDesc to calculate the tritium content.) The values plotted in the figure are also listed in Table 2.

Table 2. NeuSDesc estimates of yields from targets considered in this report at different deuteron bombarding energies. Values are for the fluence in neutrons cm^{-2} s^{-1} at 0° and 1 m from the target for a 1 μA deuteron beam.

Beam energy (keV)	500	600	800	1000	~1270	~2620
Neutron energy (MeV)	~15.2	~15.5	~16.0	~16.5	17	19
Target thickness (μg cm-2)	Fluence rate, neutrons cm^{-2} s^{-1} μA^{-1} at 0° and 1 m					
614	422	278	166	121	96.1	74.2
943	577	307	161	113	85.3	65.8
1500	1900	2060	830	472	308	237

The three plots thus give an indication of the expected 0° neutron yields per μA of beam at the chosen date for these three targets. Calculations with these T:Ti ratio would give a slightly distorted picture of the neutron spectral distributions, but give a good indication of the yields.

Despite the greater titanium thickness of the 943 μg cm^{-2} target compared to the 614 μg cm^{-2} target the yields, particularly at the higher deuteron energies, are very similar. This is because of the higher T:Ti ratio in the newer 614 μg cm^{-2} target at the date considered. For the 1500 μg cm^{-2} target the yield is a maximum at the point where the beam just stops in the titanium layer. As the deuterium beam energy decreases beyond this point the yield decreases because the deuterons do not traverse the full thickness of the titanium layer.

3. Variation of mean neutron energy, energy width, and yield, with angle

The different titanium thicknesses and tritium concentrations in the three targets mean that the properties of the neutron fields produced by these targets at different angles to the deuteron beam will

[a] For some of the older tritium targets at NPL there is evidence that the tritium content falls faster than would be expected by considering just the natural half-life, presumably due to tritium loss by heating of the target. However, there is at present no evidence of this for these three targets.

be different. Data are presented here on the variations of the neutron field with angle when the targets are bombarded with deuterons of 500 keV, 1 MeV, and the energy required to produce 19 MeV neutrons. Estimates of the characteristics at other bombarding energies can be derived by interpolation.

In Figure 9 the mean energies are plotted as a function of angle for 500 keV deuteron bombardment. At 0° the mean energy is lowest for the thickest titanium layer because of the greater energy loss of the deuteron beam traversing the layer. At backward angles the trend is reversed. At these angles the deuteron energy serves to reduce the neutron energy from the exothermic reaction, but the greater energy loss in the thicker target means that more neutrons are produced by reactions at lower deuteron energies where the effect of the deuteron energy in reducing the neutron energy is smaller.

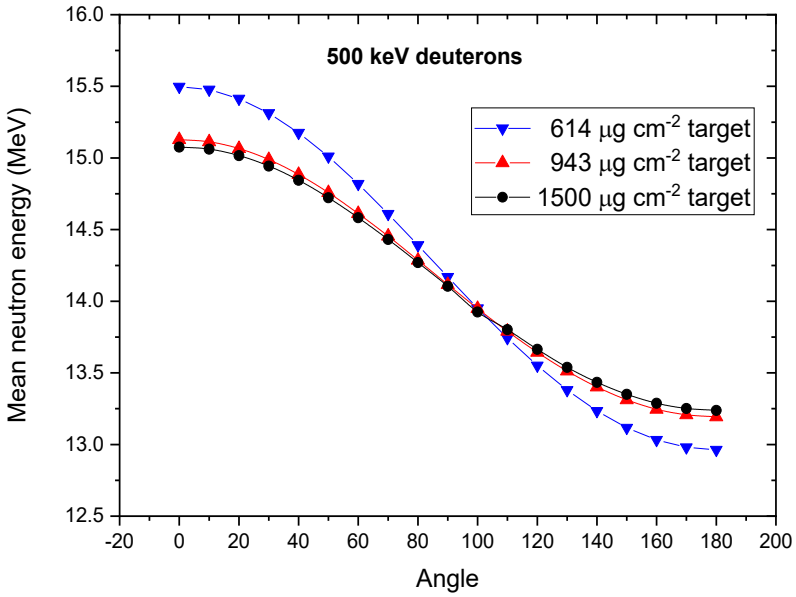

Figure 9. Variation of the mean neutron energy with angle for 500 keV deuteron bombardment.

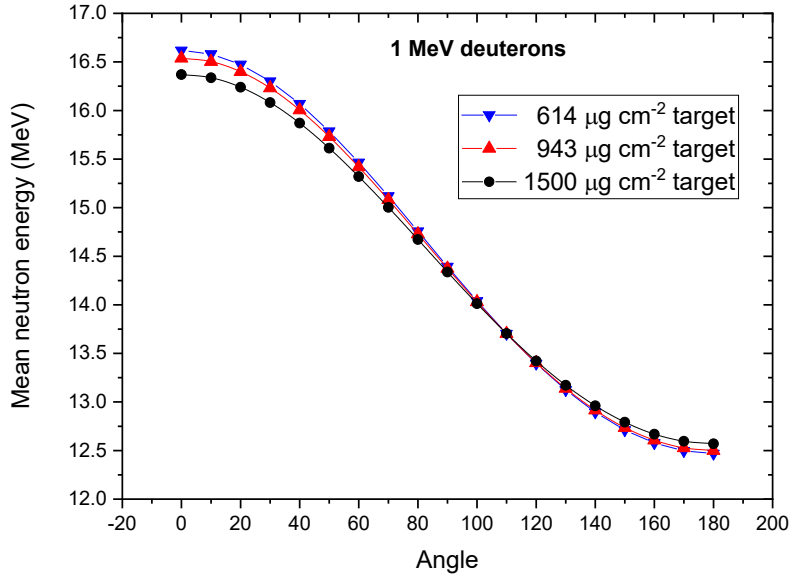

Figure 10. Variation of the mean neutron energy with angle for 1 MeV deuteron bombardment.

Figure 10 shows the mean neutron energies for the three targets for angles between 0° and 180° for bombardment with 1 MeV deuterons. The pattern of the variation with angle is very similar to that for 500 keV deuteron bombardment, with the mean energy for the 614 μg cm^{-2} target being the highest at

0° and the lowest at 180°. The differences between the mean energies are, however, smaller at this bombarding energy because of the smaller energy loss of the deuteron beam in the titanium layers.

The data for 19 MeV are shown in Figure 11. The deuteron bombarding energies were chosen for the three targets so as to produce 19 MeV neutrons at 0° and the plot, as well as illustrating how the mean energy varies with angle, shows that the same mean energies are produced at all angles for the three targets with this way of choosing the deuteron bombarding energy.

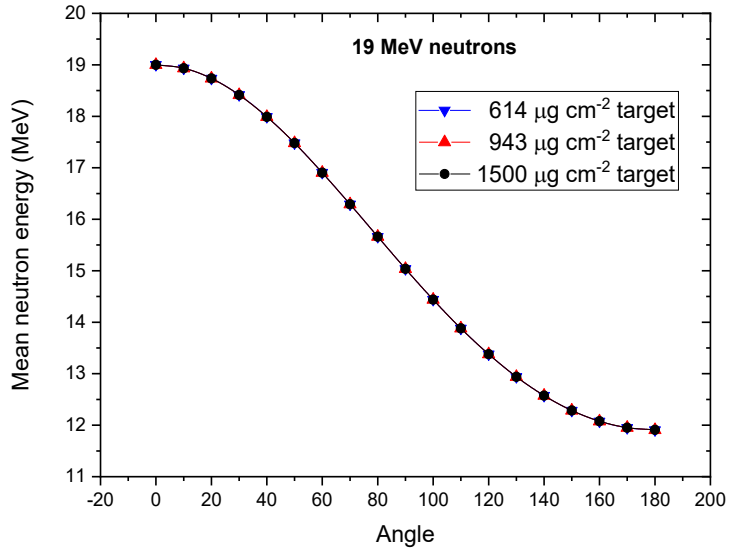

Figure 11. Variation of the mean neutron energy with angle for the production of 19 MeV neutrons.

One interesting aspect of the variation of the properties of the d-T neutron field with angle is the energy width of the neutrons. Figure 12 shows the width variations with angle for 500 keV deuteron bombardment as calculated with NeuSDesc for the three Sodern targets.

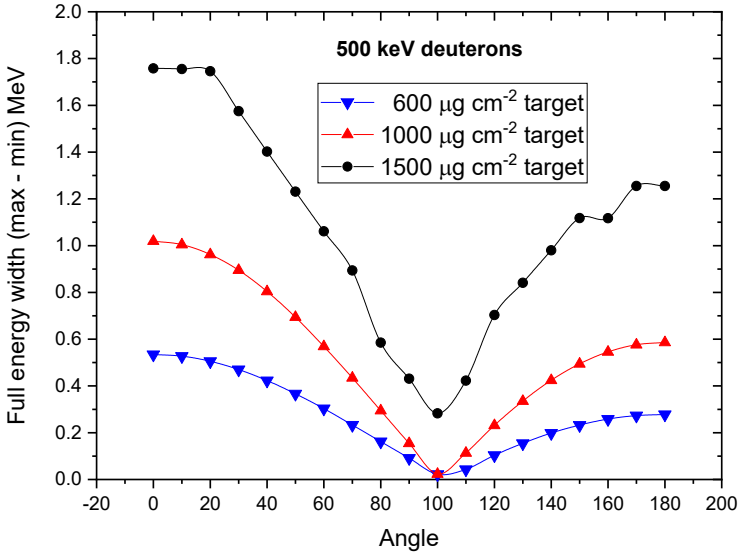

Figure 12. Full energy width of the neutron distribution as a function of angle for 500 keV deuteron bombardment.

The quantity plotted, described as the full energy width, is the value given by NeuSDesc for the difference between the maximum and minimum energy produced. A figure such as the full width at half maximum might be smaller, but the distributions are almost rectangular for high deuteron energies, and very asymmetric for lower deuteron energies, see Figures 2 to 4. The values from NeuSDesc for the

1500 μg cm^{-2} target where the beam stops in the titanium layer are not particularly smooth at large angles. This may be a limitation in the program.

The width depends of course on the titanium layer thickness, increasing with increasing thickness it has a maximum value at 0°. At this angle, the deuteron energy adds to the energy the neutron derives from the exothermic nature of the T(d,n) reaction. This additional energy is a maximum for neutron production at the surface of the titanium layer, and a minimum where the deuteron beam exits the target layer after losing energy in the titanium layer, or at the end of the track if the deuterium stops in the target layer. For backward angles the effect is reversed. The deuteron energy must be subtracted from that available to the neutron from the reaction Q value, so the highest neutron energies correspond to the lowest deuteron energies, and the lowest neutron energy results from the reactions occurring at the surface of the titanium layer where the deuteron energy is highest. Because of the reversal of the influence of the deuteron energy, the neutron energy width would be expected to have a minimum at some point when varying the angle from 0° to 180°. From Figure 12 this minimum occurs at 100° for 500 keV deuteron bombardment where the energy width becomes very narrow. For 1 MeV deuteron bombardment the energy widths are much narrower at all angles, and the minimum is now at about 110°. The values are shown in Figure 13.

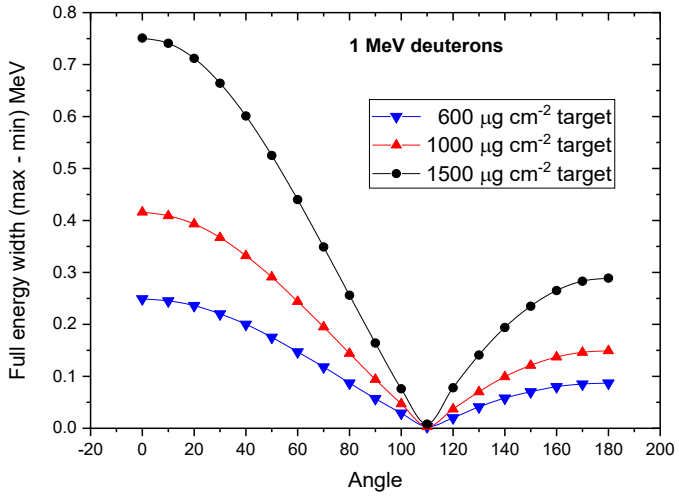

Figure 13. Full energy width of the neutron distribution as a function of angle for 1 MeV deuteron bombardment.

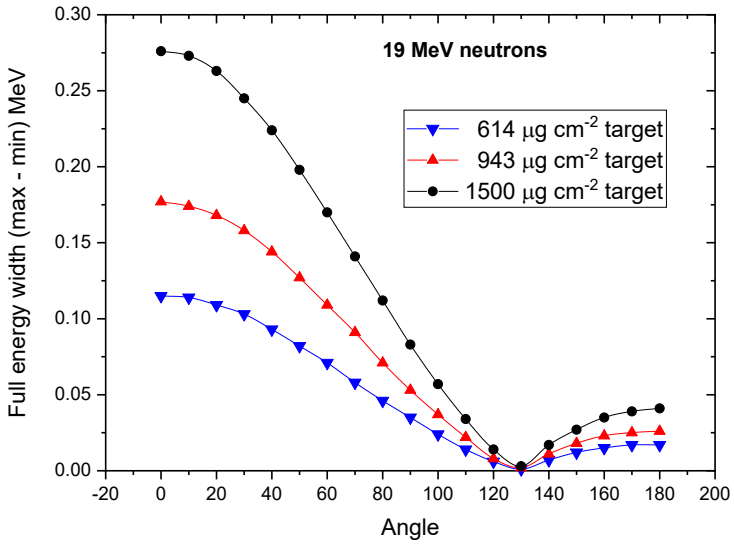

Figure 14. Full energy width of the neutron distribution as a function of angle for production of 19 MeV neutrons

For the production of 19 MeV neutrons the energy width is even narrower, and the minimum has moved up to about 130° – see Figure 14. The neutron energy at this angle is about 13 MeV.

The neutron fluences as a function of angle for the three targets are plotted in Figure 15 for 500 keV deuteron bombardment, in Figure 16 for 1 MeV deuteron bombardment, and in Figure 17 for the production of 19 MeV neutrons. They are all for a 1 μA deuteron beam.

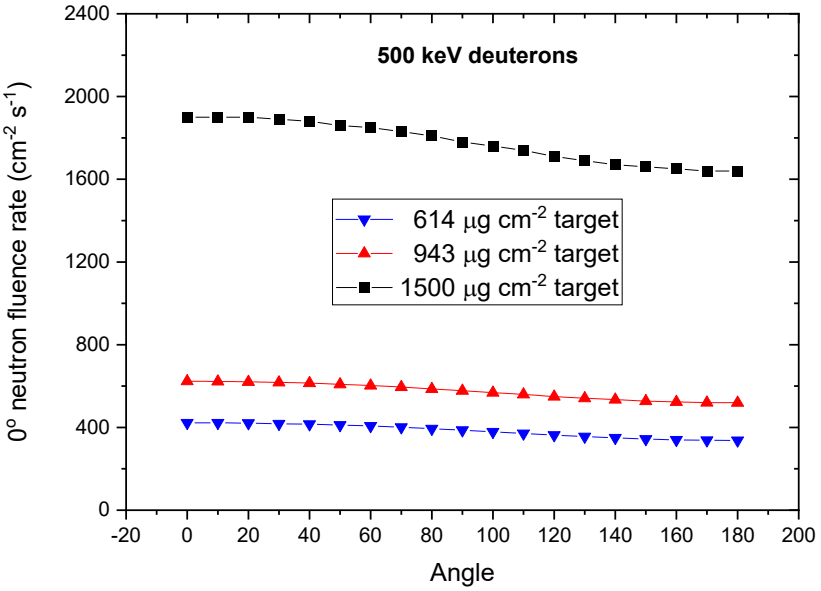

Figure 15. Neutron fluences as a function of angle of emission for 500 keV deuteron bombardment.

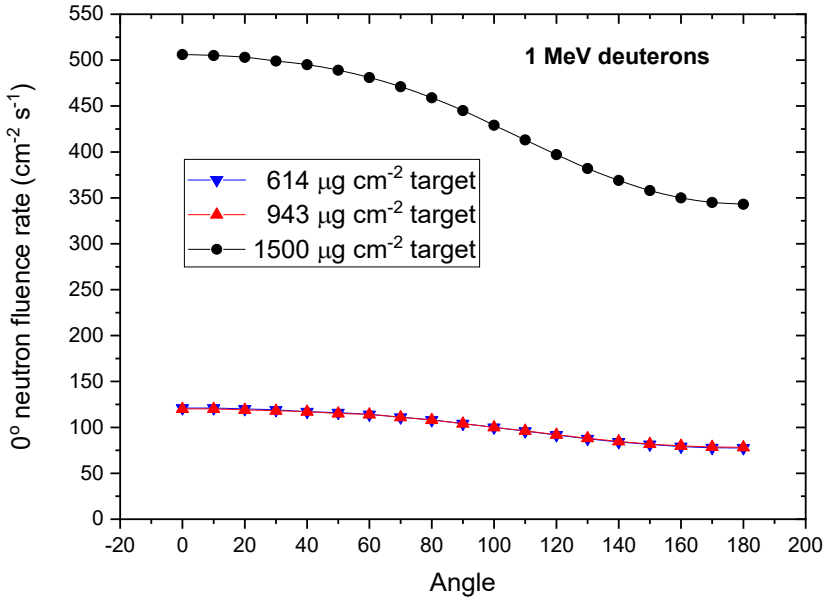

Figure 16. Neutron fluences as a function of angle of emission for 1 MeV deuteron bombardment.

The fluences depend on the reaction cross-section for each energy, the titanium layer thickness, and hence the amount of tritium in the layer, but also depend on the age of the target. The 943 μg cm^{-2} target is much older than the 614 μg cm^{-2} target so despite the greater titanium thickness of the 943 μg cm^{-2} target the yields are rather similar. The yield from the 943 μg cm^{-2} target are higher than those from the 614 μg cm^{-2} target for 500 keV deuteron bombardment. This is because the greater slowing down of the deuteron beam at this energy means that the average energy of the deuterons in the 943 μg cm^{-2} target are closer to the peak in the T(d,n) cross section. The yields are practically identical for 1 MeV neutron bombardment, and the 614 μg cm^{-2} target yield is marginally the higher of the two for 19 MeV neutron production – see Figure 17.

The yield from the 1500 μg cm^{-2} target at 19 MeV is higher than from the others. This is at an energy where the yield is low. The fact that the energy width is not large at this energy makes this target an obvious candidate for neutron production at this energy.

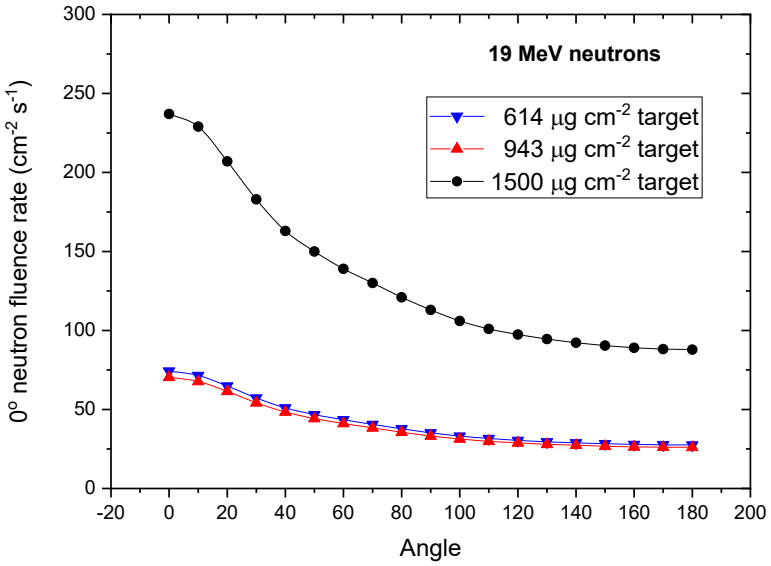

Figure 17. Neutron fluences as a function of angle of emission for 19 MeV neutron production.

One feature that is clear from the figures is that the neutron yield as a function of angle is not hugely anisotropic; the fluence does not decrease by a large amount on going to backward angles although the decrease is larger at higher deuteron energies.

4. Conversion coefficients from fluence to the operational quantities

The usual way of determining fluence to operational quantity conversion coefficients at NPL, for d-T neutron fields, has been to calculate the energy loss of the deuteron beam in the target, and to derive the coefficients for neutron energy produced by a deuteron energy half-way between the maximum and minimum values in the target layer. For the reasonably thin targets, and high deuteron energies used to date (about 1 MeV), this approach is valid, but for lower energy deuteron beams and thicker targets, where the neutron spectrum is broader, it may not be.

Conversion coefficients have been calculated here for ambient dose equivalent, and for personal dose equivalent at the angles for which conversion coefficient tables are available, for the neutron spectra produced for the thickest and thinnest targets available at NPL, for deuteron energies of 500 keV and 1 MeV. They were calculated in three different ways.

1. The conversion coefficients tabulated in ICRU 57[(5)] were interpolated to the mean energies of the bins in which NeuSDesc calculated the group-averaged spectrum. The fluence per bin was multiplied by the conversion coefficient at the mean energy and summed. This sum was then divided by the total fluence to give the spectrum averaged conversion coefficient.
2. The conversion coefficient was derived by interpolating the ICRU 57 tables to find the value at the mean neutron energy of the spectrum. This energy is a number provided by NeuSDesc.
3. The conversion coefficient was determined by calculating the neutron energy corresponding to the mean deuteron energy in the target and then interpreting the ICRU 57 data to find the coefficient corresponding to this neutron energy. This is the approach which has been used up until now at NPL.

The results are shown in Table 3 to Table 6 for a 614 μg cm^{-2} and for a 1500 μg cm^{-2} target, for 550 keV and 1 MeV deuteron beams.

Table 3. Conversion coefficients calculated for a 614 μg cm^{-2} T:Ti target bombarded with a 500 keV deuteron beam. The 'Difference' rows are to the results obtained by integrating over the spectrum.

			Mean neutron energy	15.498	MeV		
			Mean deuteron energy	377	keV		
			Neutron energy for mean deuteron energy	15.556	MeV		
	$h^*(10)$	$h_p(10,0°)$	$h_p(10,15°)$	$h_p(10,30°)$	$h_p(10,45°)$	$h_p(10,60°)$	$h_p(10,75°)$
From integration over spectrum	548.02	570.18	571.17	590.63	581.62	586.25	527.66
From mean energy of spectrum	548.10	570.21	571.20	590.66	581.64	586.29	527.68
Difference to spectrum calculation	0.01%	0.01%	0.00%	0.00%	0.00%	0.01%	0.00%
For neutron energy at mean deuteron energy	548.96	570.90	571.89	591.5441	582.39	587.10	528.55
Difference to spectrum calculation	0.17%	0.13%	0.13%	0.13%	0.13%	0.14%	0.17%

Table 4. Conversion coefficients calculated for a 614 μg cm^{-2} T:Ti target bombarded with a 1.0 MeV deuteron beam. The 'Difference' rows are to the results obtained by integrating over the spectrum.

			Mean neutron energy	16.181	MeV		
			Mean deuteron energy	923	keV		
			Neutron energy for mean deuteron energy	16.623	MeV		
	$h^*(10)$	$h_p(10,0°)$	$h_p(10,15°)$	$h_p(10,30°)$	$h_p(10,45°)$	$h_p(10,60°)$	$h_p(10,75°)$
From integration over spectrum	560.26	582.91	583.24	604.48	595.57	601.09	544.11
From mean energy of spectrum	560.27	582.92	583.25	604.49	595.58	601.10	544.11
Difference to spectrum calculation	0.00%	0.00%	0.00%	0.00%	0.00%	0.00%	0.00%
For neutron energy at mean deuteron energy	560.30	582.97	583.29	604.54	595.63	601.16	544.18
Difference to spectrum calculation	0.01%	0.01%	0.01%	0.01%	0.01%	0.01%	0.01%

Table 5. Conversion coefficients calculated for a 1500 μg cm^{-2} T:Ti target bombarded with a 500 keV deuteron beam. The 'Difference' rows are to the results obtained by integrating over the spectrum.

			Mean neutron energy	15.077	MeV		
			Mean deuteron energy	250	keV		
			Neutron energy for mean deuteron energy	15.238	MeV		
	$h^*(10)$	$h_p(10,0°)$	$h_p(10,15°)$	$h_p(10,30°)$	$h_p(10,45°)$	$h_p(10,60°)$	$h_p(10,75°)$
From integration over spectrum	540.99	564.87	565.94	585.00	575.99	579.98	521.09
From mean energy of spectrum	541.33	564.99	565.98	585.04	576.04	580.17	521.21
Difference to spectrum calculation	0.06%	0.02%	0.01%	0.01%	0.01%	0.03%	0.02%
For neutron energy at mean deuteron energy	544.03	567.03	568.01	587.22	578.21	582.57	523.73
Difference to spectrum calculation	0.56%	0.38%	0.36%	0.38%	0.39%	0.45%	0.51%

Table 6. Conversion coefficients calculated for a 1500 μg cm^{-2} T:Ti target bombarded with a 1.0 MeV deuteron beam. The 'Difference' rows are to the results obtained by integrating over the spectrum.

			Mean neutron energy	16.370	MeV		
			Mean deuteron energy	803	keV		
			Neutron energy for mean deuteron energy	16.406	MeV		
	$h^*(10)$	$h_p(10,0°)$	$h_p(10,15°)$	$h_p(10,30°)$	$h_p(10,45°)$	$h_p(10,60°)$	$h_p(10,75°)$
From integration over Spectrum	558.27	580.18	580.80	601.53	592.58	597.90	540.49
From mean energy of spectrum	558.37	580.22	580.87	601.58	592.62	597.95	540.53
Difference to spectrum calculation	0.02%	0.01%	0.01%	0.01%	0.01%	0.01%	0.01%
For neutron energy at mean deuteron energy	558.66	580.62	581.22	602.01	593.05	598.41	541.05
Difference to spectrum calculation	0.07%	0.08%	0.07%	0.08%	0.08%	0.09%	0.10%

It can be seen from the tables that the differences between the three approaches are negligible except for the thickest target, 1500 μg cm^{-2}, and the lowest deuteron energy, 500 keV, where the difference between the approach of performing a full integration over the spectrum, and simply taking the conversion coefficient for the neutron energy corresponding to the mean deuteron energy is greatest being 0.56% for ambient dose equivalent and lower for personal dose equivalent at all angles.

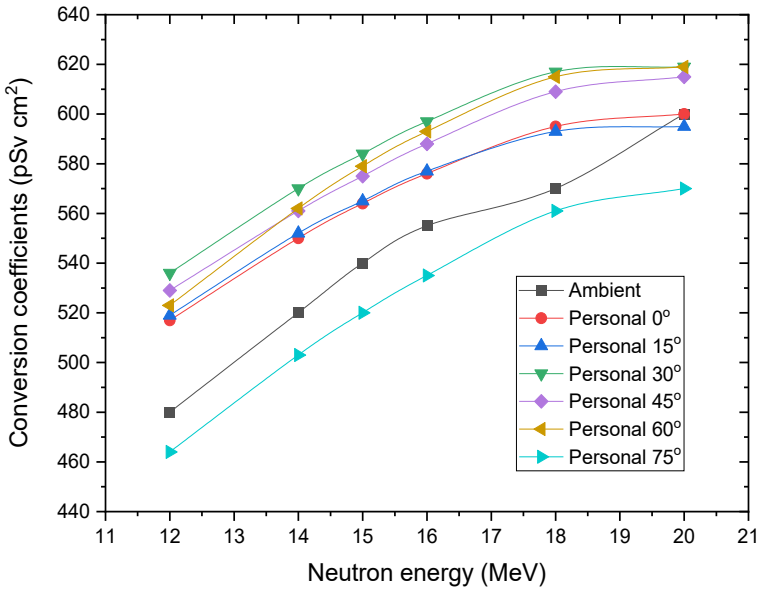

Figure 18. ICRU 57 fluence to dose equivalent conversion coefficients in the 12 to 18 MeV region.

The reason why these differences are small is explained by the variation of the conversion coefficients with neutron energy as illustrated in Figure 18. The change with energy for the rather small neutron energy differences shown in the tables is reasonably small. Either of the three approaches to deriving the conversion coefficient can be adopted, although for low deuteron energies it is probably best to use the value for the mean energy of the neutron spectrum. The integration approach is more complex than required, and as shown in the tables, the use of the mean neutron energy gives a value that is almost identical.

No tables are included for 17 MeV and 19 MeV neutrons where the differences between the three approaches to calculating the coefficients will be even smaller in view of the narrower neutron energy distributions for these energies.

5. Energy straggling of deuterons in the target layer

The track of a charged particle slowing down in a medium is not completely straight, particularly at the end of its range, and this so-called 'straggling' results in different trajectories for different particles, and this affects the neutron energy spectrum produced by deuterons slowing down in a tritium target. The code NeuSDesc has an option to allow for this straggling by linking to the SRIM code[6]. This is a freely available set of programs for calculating ranges and stopping powers for a variety of particles slowing down in a number of different materials by simulating the stopping using Monte Carlo calculations. Because the width of the neutron energy distribution at 0° is dominated by the effect of the energy loss of the deuteron traversing the target layer, the effect of straggling for the targets considered in this report is predominantly to smooth out the low energy edge of the spectrum removing the sharp low-energy cut-off without significantly altering the overall shape. Because the use of this option slows down the running of NeuSDesc considerably, so that calculations take much longer, it was not used for the majority of the calculations presented here.

The differences introduced when SRIM is used are shown in Figure 19 where neutron spectra are shown for bombarding the 943 μg cm^{-2} target with 600 keV or 1.0 MeV deuterons. The effects of the straggling

become more pronounced as the energy loss in the target increases so the effect on the neutron spectrum shape is greater for the 600 keV bombardment than for the 1.0 MeV bombardment, but in neither case is the basic information about the general shape of the neutron spectrum significantly affected by ignoring the modifications introduced by including SRIM.

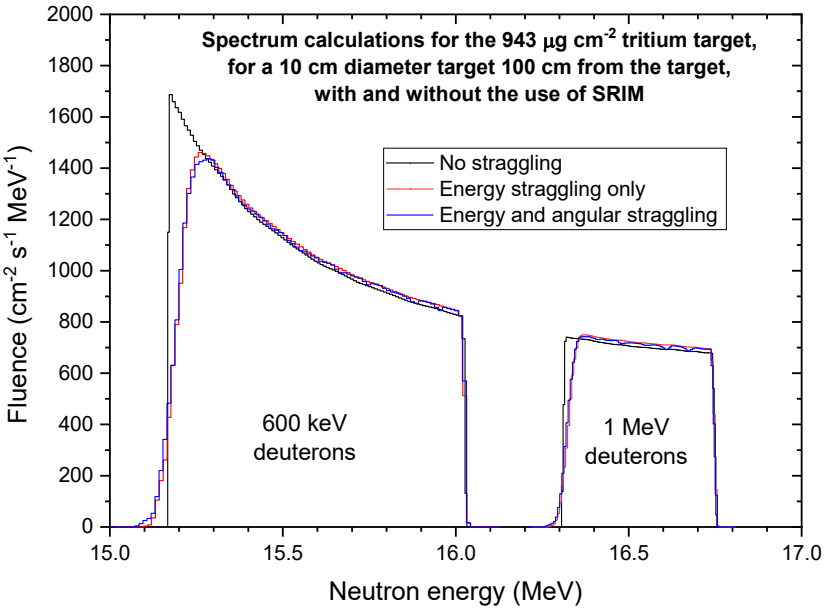

Figure 19. The effect of including energy straggling using the SRIM code when running NeuSDesc

The slowing down process affects both the deuteron energy at points along its track, called energy straggling, and the direction of travel, called angular straggling. NeuSDesc has options for including just the energy straggling, and also for including both energy and angular straggling. In Figure 19 the results for these two options are compared with the no straggling case. Although the inclusion of angular scattering does increase the number of neutrons at the lowest energy slightly, the effect is small.

The change in spectrum shape results in a small change in the neutron mean energy. Table 7 shows the changes corresponding to the two spectra shown in Figure 19. The 'Difference' columns are for differences between the with scattering and the without scattering numbers. Even for a 600 keV beam on the 943 μg cm^{-2} target the change is only 0.12%.

Table 7. The effect of using SRIM on the mean energy of the neutron distribution

Deuteron beam energy	Mean neutron energy (MeV)			Mean neutron energy (MeV)	
	No straggling	Energy straggling	Difference	Energy and angular straggling	Difference
600 keV	15.5447	15.5630	0.12%	15.5617	0.11%
1.0 MeV	16.5268	16.5326	0.04%	16.5310	0.03%

6. Utilisation of the minimum in the neutron energy width

The attraction of an angle where the neutron energy width is very narrow is that it can be used to investigate the resolution of detectors, such as diamond detectors, which produce line spectra when irradiated with monoenergetic neutrons in the 14 MeV region, or scintillators. However, when the effect of the variation of the deuteron bombarding energy as it slows down in the target on the neutron energy width is at a minimum, two other effects come into play and need to be considered. These are: the finite angle subtended by any device under investigation, and the effects of energy and angular straggling.

The first effect arises because the energy varies with angle, and thus over the face of any detector other than a point one. This effect is a minimum at 0° where the energy variation with angle is small, but is more important at other angles. The effect of straggling becomes more evident as the neutron energy width due to the energy loss of the bombarding particle in the target layer becomes small. Both effects are thus important at the angles shown in figures 11 to 13 where the neutron energy width for a point source, and ignoring scattering, are very narrow.

The effects of finite detector size are illustrated in Figure 20. This shows the neutron energy distribution for a 10 cm diameter detector and a 2 mm diameter detector at two different distances from the neutron target. The calculations are for the 1500 µg cm^{-2} target bombarded with 1 MeV deuterons with the measuring device at an angle of 109° where the effect of the target thickness is a minimum. The spectra are plotted as neutrons per cm^2 per MeV, but have all been normalised to unit total fluence. The increase in the neutron energy width as the solid angle subtended by the detector increases is clearly shown.

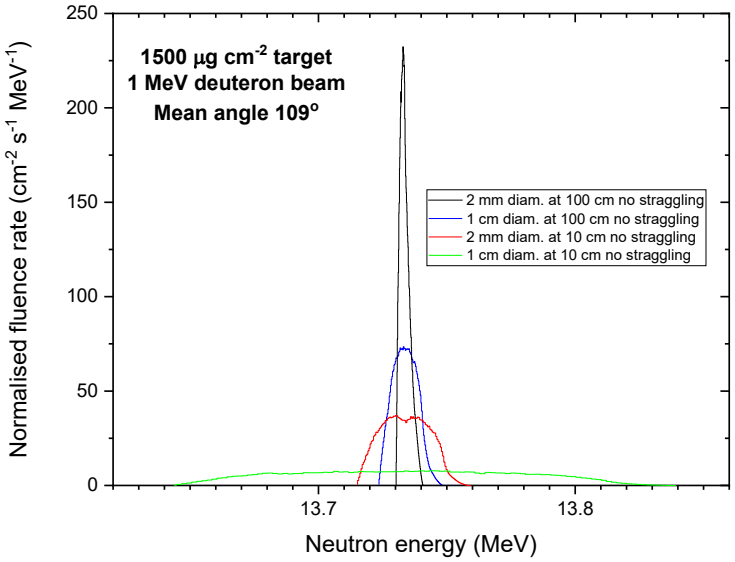

Figure 20. Neutron energy width variation with detector solid angle for a 1500 µg cm^{-2} neutron-producing Ti-T target for an angle of 109°.

Figure 21 illustrates the broadening effect of including the straggling for this rather thick target layer and the bombarding energy of 1 MeV.

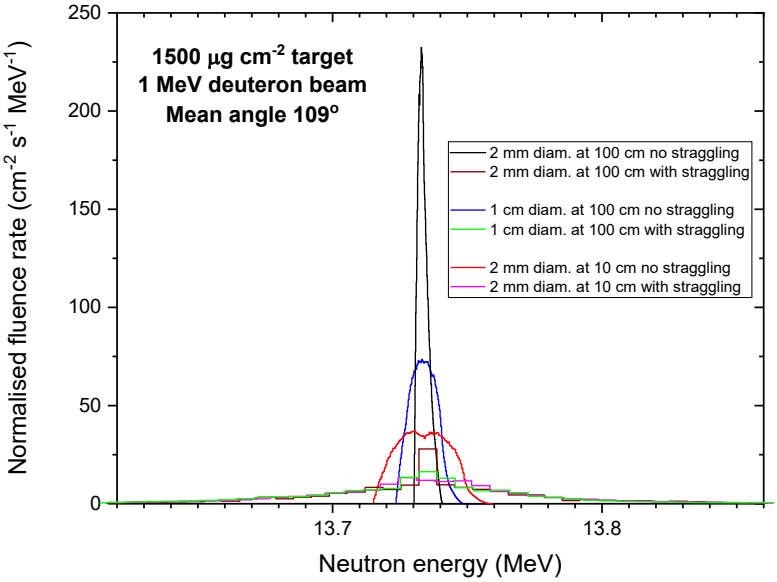

Figure 21. Neutron energy widths for a 1500 µg cm^{-2} neutron-producing Ti-T target for an angle of 109° with and without energy and angle straggling.

The significant additional energy spread introduced by the straggling is predominantly the result of the angular straggling. Energy straggling is not a significant contributor to the neutron energy width at this angle. This should not be surprising because it is the lack of dependence of the neutron energy on the deuteron energy that results in the narrow energy width at this angle.

To reduce the effect of straggling thinner targets and higher deuteron energies can be used, but both of these effects reduce the fluence. Figure 22 shows similar results to Figure 21, but for a 614 μg cm^{-2} target and a 2 MeV deuteron beam where the energy width minimum occurs at 122°. The broadening brought about by straggling is less evident for this target and energy, and for the solid angles subtended by a 1 cm diameter detector at 100 cm from the target, or a 2 mm detector at 10 cm from the target the energy width introduced by the finite solid angle dominates.

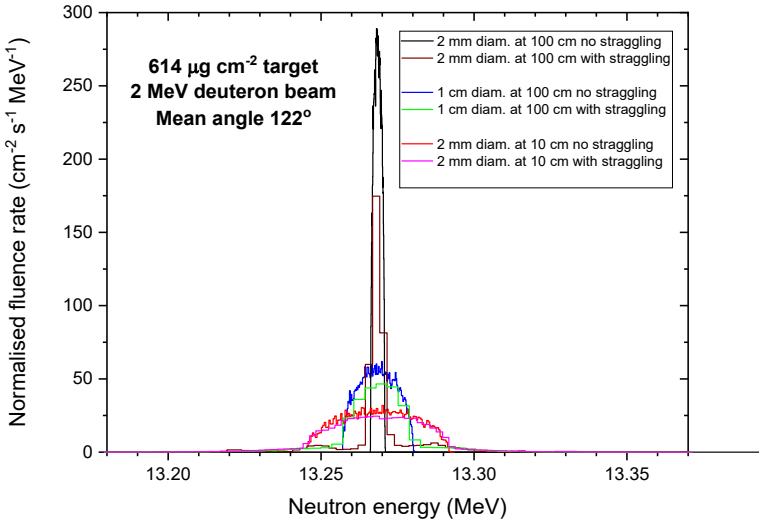

Figure 22. Neutron energy widths for a 614 μg cm^{-2} neutron-producing Ti-T target for an angle of 122° with and without energy and angle straggling.

Table 8 presents values for the energy widths of some of the distributions shown in Figure 20 to Figure 22. The flux incident on the detector for a 1 μA beam is also given. This was derived by taking the fluence rate per μA at the detector position as given by NeuSDesc, and multiplying by the detector area.

Table 8. Examples of neutron energy widths and fluxes for different diameter detectors at different distances for two tritium targets available at NPL.

1500 μg cm^{-2} target bombarded with 1 MeV deuterons								
1 cm diam. detector at 100 cm			2 mm diam. detector at 100 cm			2 mm diam. detector at 10 cm		
Peak width (keV)		Rate (s^{-1})	Peak width (keV)		Rate (s^{-1})	Peak width (keV)		Rate (s^{-1})
No scattering	With scattering		No scattering	With scattering		No scattering	With scattering	
25	576	312	11	656	12	44	591	1248
614 μg cm^{-2} target bombarded with 2 MeV deuterons								
1 cm diam. detector at 100 cm			2 mm diam. detector at 100 cm			2 mm diam. detector at 10 cm		
Peak width (keV)		Rate (s^{-1})	Peak width (keV)		Rate (s^{-1})	Peak width (keV)		Rate (s^{-1})
No scattering	With scattering		No scattering	With scattering		No scattering	With scattering	
24	193	45	5	202	2	47	180	180

Values for the widths should be treated with some caution. They are the difference between the maximum and minimum energies tabulated by NeuSDesc, rather than an estimate of a full width at half maximum which might be a more useful figure if the distributions approximated to a Gaussian shape. The energy distributions calculated with straggling tend to extend a long way from the mean although the fluence is often concentrated in a smaller region around the mean.

There is one other effect that needs to be taken into account if energy resolution measurements are attempted. The tritium in a target decays to ^{3}He, and assuming this is not lost from the target its concentration builds up; the tritium to ^{3}He ratio reaching 1:1 after a tritium half-life. Deuterons interact with ^{3}He via the ^{3}He(d,p)^{4}He reaction producing high energy protons with a total cross section in the tens of mb region for deuterons below 1 MeV[7,8]. During the only attempt to make resolution measurement for at NPL the high energy protons, energy about 14.3 MeV for a 1 MeV deuteron beam[9], traversed the thin target-can wall and were counted with 100% efficiency in the diamond detector. A thin metal shield (0.5 mm of stainless-steel plus target can wall) should be enough to remove these protons.

7. Conclusions

The neutron d-T spectral distributions that can be produced at NPL with the available targets and the deuteron beam energy range are documented. The report concentrates on the possibility of producing lower neutron energies than have been available to date, but also provides information on spectral shapes for mean neutron energies of 17 and 19 MeV. Except for the data in the last two sections all the data presented is for a point detector and do not include energy and angular straggling. They provide guidance on what d-T neutron fields are possible at NPL, but for a specific irradiation, where the effects of the finite size of the detector and straggling effects need to be considered. NeuSDesc should be run prior to performing the irradiation to check that the field energy distribution is appropriate and the yield acceptable.

The obvious features, i.e., lower mean neutron energies and a wider energy width with lower deuteron energies, are quantified. Rough values of the expected 0° yields are given for June 2022.

Both the energy data and the yield data are compromised to some extent in that inexact details of the target layer had to be used and two different T:Ti ratios are used at different points in this report.

For calculating the energy parameters, it was assumed that ^{3}He produced in the decay of tritium remains in the target layer, and that its stopping power is similar to that of tritium. (There is evidenced that the ^{3}He remains in the target layer from the fact that ^{3}He(d,p)^{4}He protons have been seen.) The T:Ti ratio of the targets when new were therefore used for these calculations.

To calculate yields in June 2022 the T:Ti ratio applicable to the targets in June 2022 were used. These are lower than the ratio when the target was first acquired due mainly to the decay of the tritium. Two effects contribute to uncertainty in these results. The first is uncertainty in the tritium concentration for the older targets because of possible losses, over and above tritium decay, resulting from beam heating. The second arises because the absence of any ^{3}He in the layer when performing the calculations means the slowing down spectrum is not absolutely correct. These effects are, however, expected to be minor.

Options for calculating neutron spectrum averaged fluence to dose equivalent conversion coefficients are also investigated with the conclusion that this important parameter in dosimetry is relatively insensitive to the method of calculation.

This report gives guidance on the characteristics of neutron fields produced using the T(d,n)^{4}He reaction at NPL, but obviously cannot cover all options. One clear conclusion from this work is that for any new irradiation, i.e. one with target and beam parameters not previously used, NeuSDesc should be run and the results studied prior to performing the irradiation to check that the field energy distribution is appropriate, and the yield acceptable.

References

1 International Organization for Standardization, *Reference neutron radiations — Part 1: Characteristics and methods of production*, ISO Standard 8529-1 2001.

2. Evert Birgersson and Göran Lövestam, *NeuSDesc – Neutron Source Description Software Manual*, JRC Scientific and Technical Report EUR 23794 EN - 2009 available from: https://publications.jrc.ec.europa.eu/repository/handle/JRC51437 .

3 H. Liskien and A. Paulsen, *Neutron Production Cross Sections and Energies for the Reactions T(p,n)^{3}He, D(d,n)^{3}He, and T(d,n)^{4}He,* Nuclear Data Tables **11** (1973) 569-619.

4 M. Drosg, *Improved Evaluation of the Differential Cross Sections of the ^{3}H(d,n)^{4}He Reaction for Deuterium Energies between 3 and 7 MeV,* Z. Phys. A – Atoms and Nuclei **300** (1981) 315-317.

5 International Commission on Radiation Units and Measurements, *Conversion Coefficients for use in Radiological Protection Against External Radiation*, ICRU Report **57**, 1998.

6 J. F. Ziegler and J. P. Biersack, SRIM-2008. Available from: http://www.srim.org.

7 K. Kudo, T. Michikawa, and T. Kinoshita, *Contribution of Fast Protons Produced by the ^{3}He(d,p)^{4}He Reactions in the Neutron Field of a T(d,n)^{4}He Source,* Nucl. Instrum. & Meths in Phys. Research **B12** (1985) 135-136.

8 M. Nocente, G. Gorini, J. Källne, and M. Tardocchi*, Cross section of the d + ^{3}He → α + p reaction of relevance for fusion plasma applications,* Nucl. Fusion **50** (2010) 055001.

9 Program for calculating reaction kinematics. Available on-line at: http://personal.ph.surrey.ac.uk/~phs1wc/kinematics/catkin2.03-installation.html.